Available online at www.sciencedirect.com
SCIENCE DIRECT®
Journal of Computational Physics 211 (2006) 513–530
JOURNAL OF COMPUTATIONAL PHYSICS
www.elsevier.com/locate/jcp

Implementation of arbitrary inner product in the global Galerkin method for incompressible Navier–Stokes equations

Alexander Yu. Gelfgat *

School of Mechanical Engineering, Faculty of Engineering, Tel-Aviv University, Ramat Aviv 69978, Israel

Received 23 February 2005; received in revised form 5 June 2005; accepted 8 June 2005
Available online 26 July 2005

Abstract

The global Galerkin or weighted residuals method applied to the incompressible Navier–Stokes equations is considered. The basis functions are assumed to be divergence-free and satisfy all the boundary conditions. The method is formulated for an arbitrary inner product, so that the pressure cannot be eliminated by Galerkin projections on a divergence-free basis. A proposed straightforward procedure for the elimination of the pressure reduces the problem to an ODE system without algebraic constraints. To illustrate the applicability and the robustness of the numerical approach and to show that numerical solutions with unit and non-unit weight functions yield similar results the driving lid cavity and natural convection benchmark problems are solved using the unit and Chebyshev weight functions. Further implications of the proposed Galerkin formulation are discussed.

Keywords: Incompressible flow; Navier–Stokes equations; Spectral methods; Chebyshev polynomials; Hydrodynamic stability

1. Introduction

This study addresses the global Galerkin or weighted residuals method for the incompressible Navier–Stokes equations, when the weight function defining the inner products is arbitrary. Assuming that the velocity basis is divergence free, and that the basis functions satisfy all the boundary conditions, it is proposed to eliminate the pressure by a direct inverse of the pressure Poisson equation operator. After this elimination the resulting dynamical system becomes explicit and does not contain any algebraic constraints. The proposed numerical procedure is tested on several benchmark problems. Results obtained with the use of unit or Chebyshev weight function are compared.

* Tel.: +972 3 6407207; fax: +972 3 6407334.
E-mail address: gelfgat@eng.tau.ac.il.

0021-9991/$ - see front matter © 2005 Elsevier Inc. All rights reserved.
doi:10.1016/j.jcp.2005.06.002

It is well-known that the pressure gradient can be eliminated from the Navier–Stokes equations by orthogonal projections on a divergence-free velocity basis, which satisfies non-penetrating boundary conditions at all boundaries. The possibility to eliminate the pressure is considered to be one of the main advantages of global spectral methods when these are applied to the calculations of incompressible flows. A way to construct the divergent-free bases in Cartesian and cylindrical coordinates was proposed in [1–3], and the corresponding global Galerkin approach yielded benchmark-quality results for several model problems of convective [3–5] and swirling [6,7] flows. It must be emphasized, however, that the pressure is eliminated only if the inner product of two vector functions $\mathbf{u}$ and $\mathbf{v}$ is defined with a unit weight, i.e., $\langle \mathbf{u}, \mathbf{v} \rangle = \int_V \mathbf{u} \cdot \mathbf{v} \, dV$, where V is the flow region. The use of any weighted inner product, i.e., $\langle \mathbf{u}, \mathbf{v} \rangle = \int_V \rho(x_1, x_2, x_3) \mathbf{u} \cdot \mathbf{v} \, dV$, where $\rho(x_1, x_2, x_3)$ is a positive non-unit function of the coordinates, will not exclude the pressure. Thus, for example, the basis functions in [1–7] were defined using Chebyshev polynomials while the inner products there were defined with the unit, but not with the Chebyshev, weight function. This altered the orthogonal properties of the polynomials and led to dense matrices. It can be expected that the use of the Chebyshev weight in the definition of the inner products, which exploits the orthogonal properties of the polynomials and yields better resolution of boundary layers, will improve the convergence of the method. However, it will require a solution for the pressure. In the framework of spectral and pseudospectral methods the pressure is usually decoupled during numerical integration in time by, for example, the influence matrix technique [8] or by the pressure-correction projection scheme [9]. Here we propose to exclude the pressure by the direct inverse of the Galerkin projection of the pressure equation operator. This allows for a direct elimination of the pressure. Taking into account that the continuity equation and the boundary conditions are satisfied analytically by an appropriate choice of the basis functions, the pressure elimination reduces the numerical model to an explicit system of ODEs without further algebraic constraints, thus preserving the important features of the global spectral methods.

The procedure of explicit pressure elimination can be important for the development of effective pseudospectral solvers based on divergent-free bases that satisfy all the boundary conditions. Such methods were applied in [10–13]. However, the difficulties related to pressure calculation led to the use of the fourth-order stream function formulation together with the Chebyshev weight [10], or to the redefinition of the basis or trial functions in a way that leads to the elimination of the non-unit weight function, so that the unit weight is enforced [11]. Suslov and Paolucci [12,13] proposed to incorporate the Chebyshev weight into the projection system keeping the unit weight function in the inner product and making the basis and projection functions orthogonal. The possibility to eliminate the pressure explicitly can allow for development of other pseudo-spectral formulations, which will not contain any implicit pressure-calculation steps. Furthermore, if the pressure can be eliminated for an arbitrary weight function, one can adapt the weight function to a specific problem that is being considered. The problem of the adaptation of the weight function was never considered before. We illustrate this possibility for the Burgers equation in Appendix A. A similar adaptation for the Navier–Stokes equation is more complicated and is beyond the scope of present study. The numerical procedure described here is necessary to proceed further with the adaptation problem.

In the following, we describe the pressure elimination scheme and illustrate its applicability and robustness on several well-known benchmark problems. We use basis functions defined as linear superpositions of the Chebyshev polynomials [1–3] and compare results computed with the use of unit and Chebyshev weight functions in the inner products. It is emphasized that at this stage we only establish a possibility of the pressure elimination procedure by showing the similarity of results obtained using the unit and non-unit weight functions. An improvement in the computational costs will be achieved, e.g., after the weight adaptation will be carried out for a certain problem, so that one will be able to reach a desired accuracy using shorter Galerkin series.

In the following, we consider the lid-driven cavity problem and three benchmark problems related to the natural convection flows. Note, that the global Galerkin approach of [1–7] was used to analyze the linear stability of numerically calculated flows. It was concluded by different authors that such an analysis

requires a good numerical resolution of both the basic steady state flow and the most unstable perturbation that triggers the instability. Consequently, in this study we focus on the convergence of steady state flows and the critical parameters corresponding to the onset of the oscillatory instability in these flows.

2. Formulation

Consider the momentum and continuity equation describing the flow of an incompressible fluid

$$\frac{\partial \mathbf{v}}{\partial t} + (\mathbf{v}\cdot\nabla)\mathbf{v} = -\nabla p + \frac{1}{Re}\Delta\mathbf{v} + \mathbf{f}, \tag{1}$$

$$\nabla\cdot\mathbf{v} = 0, \tag{2}$$

where $\mathbf{v}$ is the velocity p the pressure, $\mathbf{f}$ the volumetric force and Re is the Reynolds number. The equation for the pressure field is derived by applying the divergence operator to (1):

$$\Delta p = -\nabla\cdot[(\mathbf{v}\cdot\nabla)\mathbf{v}] + \nabla\cdot\mathbf{f}. \tag{3}$$

The boundary conditions for the pressure are defined as in [14]:

$$\left[\frac{\partial p}{\partial n}\right]_{\Gamma} = \mathbf{n}\cdot\left[\frac{1}{Re}\Delta\mathbf{v} + \mathbf{f} - \frac{\partial \mathbf{v}}{\partial t} - (\mathbf{v}\cdot\nabla)\mathbf{v}\right], \tag{4}$$

where $\mathbf{n}$ is the normal vector to the boundary Γ. The boundary condition (4) is a limit of the component of the momentum equation normal to a boundary. It is emphasized that the use of this boundary condition for the correct determination of the pressure is crucial. We have tried simpler boundary conditions as well, however all of them led to wrong results.

Eqs. (3) and (4) define the pressure to within an additive constant. The solution can be made unique by the addition of a Dirichlet point or by fixing the value of one coefficient in the Galerkin series. Then the Laplacian operator in Eq. (3) can be inversed, and the pressure is obtained formally as

$$p = \Delta^{-1}\{-\nabla\cdot[(\mathbf{v}\cdot\nabla)\mathbf{v}] + \nabla\cdot\mathbf{f}\}, \tag{5}$$

where Δ^{-1} is the inverse Laplacian operator. Substitution of (5) into (1) yields

$$\frac{\partial \mathbf{v}}{\partial t} + (\mathbf{v}\cdot\nabla)\mathbf{v} = -\nabla\left[\Delta^{-1}\{-\nabla\cdot[(\mathbf{v}\cdot\nabla)\mathbf{v}] + \nabla\cdot\mathbf{f}\}\right] + \frac{1}{Re}\Delta\mathbf{v} + \mathbf{f}, \tag{6}$$

which defines a formal way of excluding the pressure from Eqs. (1) and (2).

The derivation of Eq. (3) from Eqs. (1) and (2) assumes that the continuity Eq. (2) is always satisfied. This is not the case for most of the numerical methods dealing with the incompressible flows, since the continuity equation is satisfied at a certain stage of the whole numerical procedure (e.g., fractional time step and projection schemes) or is satisfied only approximately throughout the numerical procedure (e.g., penalty methods). It was argued also [15] that the numerical solution of the pressure problem (3) and (4) together with the momentum equation (1) does not yield a divergence free solution for velocity. The global spectral methods with divergence-free velocity basis functions do not have this problem, because the continuity equation is satisfied analytically before the numerical process starts. Thus, any approximation of a solution is analytically divergence free. This gives a theoretical opportunity to define a numerical analog of Eq. (6), so that the pressure will be excluded from the numerical scheme.

Assume that velocity and pressure are approximated by truncated series as

$$\mathbf{v} = \sum_{i=1}^{I_v}\alpha_i(t)\mathbf{u}_i(x_1,x_2,x_3), \quad p = \sum_{i=1}^{I_p}\beta_i(t)\mathbf{q}_i(x_1,x_2,x_3), \tag{7}$$

where x_i are orthogonal coordinates, $\mathbf{u}_i$ and q_i are basis functions in the corresponding functional spaces, and $\alpha_i(t)$ and $\beta_i(t)$ are unknown time-dependent scalar coefficients. Assume also, that $\nabla\cdot\mathbf{u}_i=0$, so that the approximation of the velocity is always divergence-free. Assume additionally that the basis functions $\mathbf{u}_i$ satisfy all the velocity boundary conditions, which are assumed to be linear and homogeneous. Note that orthogonality of the basis functions is not required. Substitution of (7) in (1), (3) and (4), and projection of the residuals on the bases $\mathbf{u}_i$ and q_i, respectively, reduces the problem to a system of ordinary differential and algebraic equations, which can be expressed as

$$S_{ij}\dot{\alpha}_j = G_{ij}\beta_j + L_{ij}\alpha_j + N_{ijk}\alpha_j\alpha_k + F_i, \quad i=1,\dots,I_v, \tag{8}$$

$$Q_{ij}\beta_j = B_{ij}\dot{\alpha}_j + C_{ij}\alpha_j + M_{ijk}\alpha_j\alpha_k + R_i, \quad i=1,\dots,I_p, \tag{9}$$

Here repeating indices denote summation and the dot denotes the time derivative. Eq. (8) contain projections of Eq. (1). Eq. (9) consist partially of the projections of Eq. (3) and partially of the projections of the boundary condition Eq. (4).

The matrix Q_{ij} in Eq. (9) is the projection of the Laplacian operator of Eq. (3) with the Neumann boundary conditions (4) and the Dirichlet point mentioned above. This matrix is non-singular and can be inverted. Thus, using Eq. (9), the pressure coefficients β_i can be expressed as

$$\beta_i = Q^{-1}_{ij}\left[B_{ij}\dot{\alpha}_j + C_{ij}\alpha_j + M_{ijk}\alpha_j\alpha_k + R_i\right], \quad i=1,\dots,I_p,\ \ j,k=1,\dots,I_v. \tag{10}$$

Clearly, Eqs. (10) are projections of Eq. (5). Now, substituting β_i from (10) into Eq. (8) we obtain a system of ODEs for the velocity coefficients α_i:

$$S_{ij}\dot{\alpha}_j = G_{ij}Q^{-1}_{jm}\left[B_{mn}\dot{\alpha}_n + C_{mn}\alpha_n + M_{mkn}\alpha_k\alpha_n + R_m\right], + L_{ij}\alpha_j + N_{ijk}\alpha_j\alpha_k + F_i, \quad i,j,k,n=1,\dots,I_v,\ m=1,\dots,I_p, \tag{11}$$

which are the Galerkin projections of Eq. (6). Thus, the velocity coefficients α_i can be calculated directly from Eqs. (11) with no need of any information regarding the pressure coefficients β_i. The pressure can be obtained using Eqs. (7) and (10) after the velocity is calculated. At this stage, assuming that the velocity is calculated with a sufficient accuracy, the truncation number of the pressure Galerkin series (7) I_p can be increased, if necessary. This will require a recalculation of Eq. (9), but no recalculation of the velocity α_j will be needed.

The inner products are defined as

$$\langle f,g\rangle = \int_V \rho(x_1,x_2,x_3)f(x_1,x_2,x_3)g(x_1,x_2,x_3)\,\mathrm{d}V, \quad \rho(x_1,x_2,x_3)>0 \tag{12}$$

for scalar, and

$$\langle \mathbf{u},\mathbf{v}\rangle = \langle u_1,v_1\rangle + \langle u_2,v_2\rangle + \langle u_3,v_3\rangle \tag{13}$$

for vector functions. In the case of the unit weight function, $\rho(x_1, x_2, x_3)\equiv 1$, the matrix G_{ij} usually vanishes, since $\langle\nabla p,\mathbf{u}\rangle=0$ for any scalar function p if $\mathbf{u}$ is divergence free and satisfies non-penetration boundary conditions on all boundaries. In these cases $G_{ij}=0$ and Eq. (11) become significantly simplified. This simplified form of Eq. (11) was treated in [1–7]. The computational cost of calculations with a non-unit weight functions is connected with the calculation of the bilinear term $M_{mkn}\alpha_k\alpha_n$, which is approximately the same as calculation of another bilinear term $N_{ijk}\alpha_j\alpha_k$, which never vanishes.

In the following, we consider several benchmark problems for flows in rectangular domains $0\leqslant x\leqslant 1$, $0\leqslant y\leqslant A$. For these flows we describe the elimination of pressure using the basis functions defined in [1–3]. The velocity and the pressure are approximated by the Galerkin series

$$\mathbf{v} = \mathbf{W}(x,y) + \sum_{i=0}^{N_x}\sum_{j=0}^{N_y}\alpha_{ij}(t)\mathbf{w}_{ij}(x,y), \quad p = \sum_{i=0}^{M_x}\sum_{j=0}^{M_y}\beta_{ij}(t)T_i(x)T_j\left(\frac{y}{A}\right), \tag{14}$$

where

$$\mathbf{w}_{ij}(x,y)=\left\{\begin{array}{l}\frac{A}{2}\sum\limits_{m=0}^{4}\frac{a_{im}}{(i+m)}T_{i+m}(x)\sum\limits_{l=0}^{4}b_{jl}U_{j+l-1}\left(\frac{y}{A}\right)\\ -\sum\limits_{m=0}^{4}a_{im}U_{i+m-1}(x)\sum\limits_{l=0}^{4}\frac{b_{jl}}{2(j+l)}T_{j+1}\left(\frac{y}{A}\right)\end{array}\right\},\tag{15}$$

and T_i, U_j are Chebyshev polynomials of the first and the second kind. It can be easily shown that $\nabla\cdot\mathbf{w}_{ij}=0$ [1–3]. The coefficients a_{im} and b_{jl} are defined to satisfy the velocity boundary conditions. The expressions defining a_{im} and b_{jl} for the no-slip and stress-free boundary conditions, as well as other technical details regarding numerical implementation of the method, can be found in [1–3]. The divergence free vector function $\mathbf{W}(x,y)$ is needed to make all the boundary conditions for the functions $\mathbf{w}_{ij}$ homogeneous (see below). The basis functions $\mathbf{w}_{ij}$ defined by Eq. (15) were introduced by Gelfgat and Tanasawa [1], and are used also as the projection system in [1–7] and here. The same basis functions for the Galerkin series (14) were used by Suslov and Paolucci [12,13], however their projection system was different and incorporated Chebyshev weight to allow for the functions orthogonality and an efficient implementation of the pseudo-spectral approach.

For the convection benchmark problems we consider the Boussinesq approximation of the momentum, energy and continuity equations. The system of equations reads

$$\frac{\partial\mathbf{v}}{\partial t}+(\mathbf{v}\cdot\nabla)\mathbf{v}=-\nabla p+\nabla\mathbf{v}+Gr\theta\mathbf{e}_y,\tag{16a}$$

$$\nabla\cdot\mathbf{v}=0,\quad\frac{\partial\theta}{\partial t}+(\mathbf{v}\cdot\nabla)\theta=\frac{1}{Pr}\Delta\theta,\tag{16b, c}$$

where θ is the temperature, Gr and Pr are the Grashof and Prandtl numbers, respectively. The Galerkin approximation and the basis functions for the temperature are defined as in [1].

Below we test the pressure elimination procedure that was described above considering three different numerical cases, which are defined in the following. The ''unit weight'' case assumes that all the Galerkin projections are defined with the unit weight, so that the pressure is eliminated by the orthogonal projections on the divergence free velocity basis, i.e., $G_{ij}=0$. The ''Chebyshev weight'' case assumes that all the Galerkin projections are defined with the Chebyshev weight, which for the intervals $0\leqslant x\leqslant 1,\ 0\leqslant y\leqslant A$ read

$$\langle f,g\rangle=\int_0^A\int_0^1(x-x^2)^{-1/2}\left(\frac{y}{A}-\left(\frac{y}{A}\right)^2\right)^{-1/2}f(x,y)g(x,y)\,\mathrm{d}x\,\mathrm{d}y.\tag{17}$$

Finally, the ''mixed weight'' case assumes that the Chebyshev weight is used for the momentum equation, while the unit weight is used for the pressure equation (3) and the energy equation (16c). In all non-isothermal calculations we use equal truncations in the velocity and the temperature Galerkin series. The truncation numbers for the pressure series are defined as $M_x=N_x+4$, $M_y=N_y+4$. Our numerical experiments showed that further increase of M_x and M_y does not alter the accuracy of the calculated velocity field. It is emphasized once more that the Chebyshev weight here serves as an example of an arbitrary weight function.

Together with the formulation (1)–(3) one can consider the so-called divergent form of the momentum equation

$$\frac{\partial\mathbf{v}}{\partial t}+(\nabla\times\mathbf{v})\times\mathbf{v}=-\nabla\tilde{p}-\frac{1}{Re}\nabla\times\nabla\times\mathbf{v}+\mathbf{f},\quad\tilde{p}=p+\nabla\cdot\left(\frac{v^2}{2}\right),\tag{18}$$

which yields instead of Eqs. (5) and (6)

$$\tilde{p} = \Delta^{-1}\{-\nabla\cdot[(\nabla\times\mathbf{v})\times\mathbf{v}] + \nabla\cdot\mathbf{f}\}, \tag{19}$$

$$\frac{\partial\mathbf{v}}{\partial t} + (\nabla\times\mathbf{v})\times\mathbf{v} = -\nabla[\Delta^{-1}\{\nabla\cdot[(\nabla\times\mathbf{v})\times\mathbf{v}] + \nabla\cdot\mathbf{f}\}] - \frac{1}{Re}\nabla\times\nabla\times\mathbf{v} + \mathbf{f}. \tag{20}$$

With the use of this formulation the general form of Eqs. (8)–(11) does not change, but the matrices are composed of different inner products. Additionally, it is possible to consider the stream function formulation ($v_x = \partial\psi/\partial y$, $v_y = \partial\psi/\partial x$):

$$\frac{\partial\Delta\psi}{\partial t} - \frac{\partial\psi}{\partial x}\frac{\partial\Delta\psi}{\partial y} + \frac{\partial\psi}{\partial y}\frac{\partial\Delta\psi}{\partial x} = \frac{1}{Re}\Delta\Delta\psi + \nabla\times\mathbf{f}. \tag{21}$$

The basis functions for the stream function ψ can be easily derived from (15):

$$\psi_{ij}(x,y) = A\sum_{m=0}^{4}\frac{a_{im}}{2(i+m)}T_{i+m}(x)\sum_{l=0}^{4}\frac{b_{jl}}{2(j+l)}T_{j+l}\left(\frac{y}{A}\right). \tag{22}$$

Using Green's integral theorems it can be easily shown that for the divergent-free velocity basis functions (15) and the unit weight function, Eqs. (1), (18) and (21) yield identical Galerkin projections. However, if a non-unit weight is applied the three formulations lead to different results. Our numerical experiments with the Chebyshev weight (17) showed that the formulations (18) and (21) do not give any advantage in the convergence of the accuracy compared with the formulation (1). An example of that is given below. Clearly, this conclusion cannot be applied to other weight functions.

3. Results

3.1. Lid-driven cavity flow

One of the widely used benchmark problems is the lid-driven cavity flow (see [16–24] and references therein). The flow in a square cavity (i.e., $A = 1$) whose upper boundary moves with constant velocity is considered. The velocity boundary conditions are

$$v_x = -1, \quad v_y = 0 \ \text{ at } y = 1, \tag{23a}$$

$$v_x = v_y = 0 \quad \text{at } y = 0 \ \text{ and } x = 0, 1. \tag{23b}$$

The boundary conditions (18) are discontinuous at the upper corners of the cavity, and are not homogeneous at $y = 1$. To exclude the inhomogeneity and to smooth the discontinuity we define the divergence free function $\mathbf{W}(x,y)$ in Eq. (14) as the solution of the problem:

$$\Delta\mathbf{W} = 0, \quad W_x(x, y = 1) = (2x-1)^n - 1, \quad W_y(x, y = 1) = 0, \quad \mathbf{W}(y = 0) = \mathbf{W}(x = 0, 1) = 0. \tag{24}$$

The value of the power n is assumed to be large (in our calculations $n \geqslant 20$), so that the value of W_x at $y = 1$ is close to -1 everywhere except near the corners, where it quickly vanishes. The problem (24) is solved using the Galerkin series with $\tilde{N}_x \times N_y$ basis functions (15) with the coefficients a_{im} and b_{jl} chosen to satisfy the homogeneous boundary conditions of (24). Apparently, the condition $\nabla\cdot\mathbf{W} = 0$ is also satisfied. $\tilde{N}_x \times (N_y - 1)$ equations for calculations of the coefficients of the series of $\mathbf{W}$ are obtained by the Galerkin projections of the residual of the equation $\Delta\mathbf{W} = 0$ on the same basis functions. The remaining $\tilde{N}_x$ equations are derived from the boundary condition at $y = 1$, which is satisfied in $\tilde{N}_x$ Chebyshev collocation points at this boundary. Once the function $\mathbf{W}(x,y)$ is calculated, the boundary condition for the remaining Galerkin series in Eq. (14) are homogeneous. In the following calculations we used $\tilde{N}_x = 100$.

The calculated flow pattern for $Re = 1000$ is illustrated in Fig. 1. The calculations were done with the truncation $N = N_x = N_y = 60$, unit weight and $n = 60$ in the smoothing function (24). The pressure field

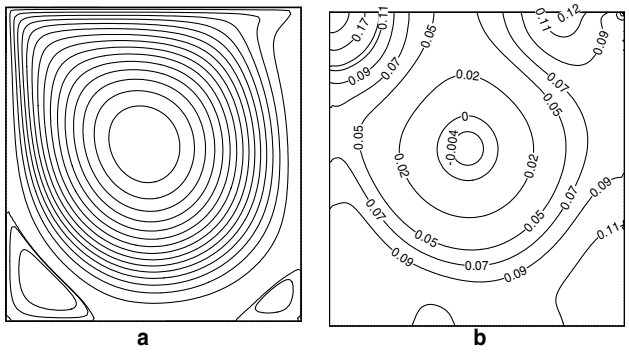

Fig. 1. Lid-driven cavity flow at $Re = 1000$. (a) Streamlines, (b) Isolines of the pressure.

is calculated using Eqs. (7) and (10) as the Galerkin projection of Eq. (5), using the calculated velocity field. The streamlines in Fig. 1(a) are equally spaced between $\psi_{\min} = -1.7281 \times 10^{-3}$ and $\psi_{\max} = 0.11886$, and three more streamlines for $\psi = 0, -0.56 \times 10^{-3}$ and -0.76×10^{-4} are added to illustrate the reverse circulations located in the lower corners. Levels of the isobars shown in Fig. 1(b) correspond to the levels shown in Fig. 3 of [16]. Comparison with that figure shows a good agreement in the pressure field calculated in both studies.

The characteristic features of the flow are compared with the results of [16] in Table 1 in terms of the maximal and minimal values of the stream function and their locations. A comparison with the very precise results of [16] shows that the solution obtained using 60×60 basis functions and unit weight is correct to within the fourth decimal digit. The calculation with the mixed weight yields the identical result. The result obtained with the use of Chebyshev weight is slightly worse. A slight difference between the present results and the results of [16] can be caused by the smoothing of the discontinuity in the boundary conditions. Apparently, different numerical methods smooth the discontinuity in different ways. This issue is discussed below in more details.

Fig. 2 shows the convergence of the critical Reynolds number and the critical circular frequency of oscillations (i.e., the imaginary part of the leading eigenvalue) corresponding to the oscillatory instability of the two-dimensional flow with respect to purely two-dimensional perturbations. The critical parameters are compared with several published results in Table 2. The calculations are done for different weight functions, as well as for different values of the smoothing parameter $n = 20$, 40 and 60. It is known that the primary instability of the lid-driven cavity flow is three-dimensional and sets in at $Re_{\mathrm{cr}} < 1000$ [17,18]. Here we are motivated by a convergence study rather than by physically meaningful results and therefore choose the

Table 1
Results of the calculation of steady lid-driven cavity flow at $Re = 1000$

Property	Present result 60×60 basis functions, $n = 60$, unit weight	Present result 60×60 basis functions, $n = 60$, mixed weight	Present result 60×60 basis functions, $n = 60$, Chebyshev weight	Result of [16] 160×160 Chebyshev polynomials
$\psi_{\max}$	0.11886	0.11885	0.11890	0.1189366
$x_{\max}$	0.4691	0.4691	0.4691	0.4692
$y_{\max}$	0.5652	0.5652	0.5652	0.5652
$\psi^{(1)}_{\min}$	-1.7281×10^{-3}	-1.7281×10^{-3}	-1.7254×10^{-3}	-1.729717×10^{-3}
$x^{(1)}_{\min}$	0.1359	0.1359	0.1360	0.1360
$y^{(1)}_{\min}$	0.1118	0.1118	0.1117	0.1118
$\psi^{(2)}_{\min}$	-2.3317×10^{-4}	-2.3335×10^{-4}	-2.3525×10^{-4}	-2.334528×10^{-4}
$x^{(2)}_{\min}$	0.9167	0.9167	0.9164	0.9167
$y^{(2)}_{\min}$	0.07809	0.07810	0.07805	0.07810

purely two-dimensional instability, for which the critical Reynolds number is approximately 8000 [19–24] and the calculations are more difficult. As noted above, the convergence of the critical parameters means the convergence of both the steady state flow and the leading eigenvalues/eigenvectors of the linearized stability problem.

The results reported in Fig. 2 and Table 2 show that the critical parameters depend on the choice of the weight functions and smoothing of the boundary conditions. The difference is caused, in particular, by the different weight function used for the solution of (24). The resulting function **W** is slightly different when it is calculated using the unit or Chebyshev weight. This difference is caused by the sharp change of the function, even when it is smoothed, near the upper right corner of the cavity. This difference causes a slight difference in the calculated steady flow state at $Re = 1000$, which can be seen in the fourth decimal digit (Table 1). A more pronounced difference is observed, as expected, when the calculation is carried out for a significantly larger critical Reynolds number. Fig. 2 shows that the difference between the critical parameters cal-

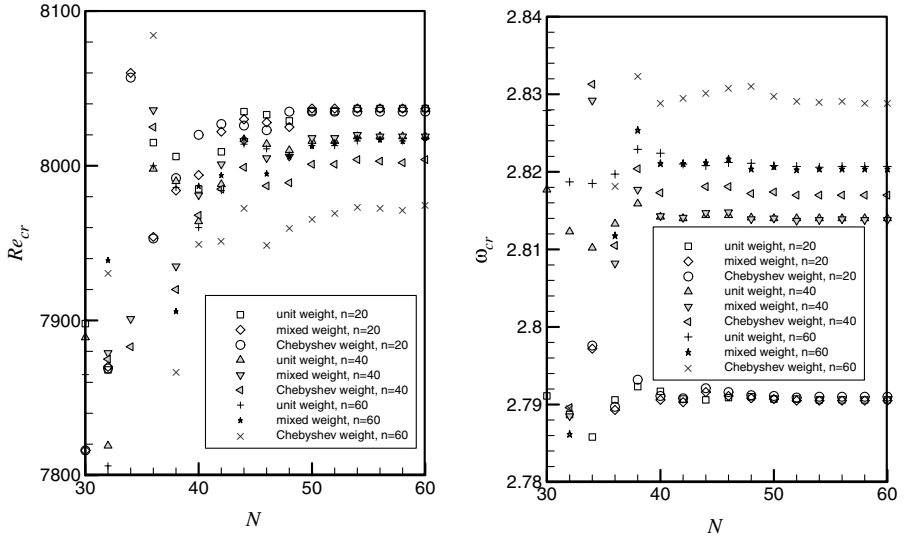

Fig. 2. Lid-driven cavity flow. Convergence of the critical Reynolds number and the critical frequency for different weight functions and different smoothing parameter n. $N = N_x = N_y$.

Table 2
Critical Reynolds number and critical oscillation frequency for lid-driven cavity flow

Reference	Discretization	Re_{cr}	ω_{cr}
[19]	57×57 finite biquadratic elements	7763.4	2.8634
[20]	Unstructured finite element grid with 27890 degrees of freedom	8040	2.829
[21]	60×60 finite biquadratic elements	8000	2.8356
[22]	160×160 Chebyshev collocation points	8018	2.8249
[23]	200×200 uniform grid	7704	3.707
[24]	257×257 stretched grid	8069.76	2.8251
Present			
$n = 20$, unit weight	60×60 basis functions	8037	2.791
$n = 20$, Chebyshev weight	60×60 basis functions	8036	2.791
$n = 40$, unit weight	60×60 basis functions	8019	2.814
$n = 40$, Chebyshev weight	60×60 basis functions	8004	2.817
$n = 60$, unit weight	60×60 basis functions	8017	2.821
$n = 60$, Chebyshev weight	60×60 basis functions	7975	2.829

culated with different weights also increases with increasing n, i.e., when the smoothing function in (24) becomes steeper. This is a clear sign of the occurrence of the Gibbs phenomenon near the corner. Apparently, the Gibbs phenomenon is more pronounced for the Chebyshev weight, which grows sharply near the boundaries. Thus, we conclude that the calculation of the function **W** using the unit weight is preferable.

Fig. 2 shows that the unit and mixed weight functions yield almost identical results, while the use of the Chebyshev weight everywhere leads to slightly different results. When the discontinuity of the boundary condition is strongly smoothed, i.e., $n = 20$, there is no visible difference in the convergence rate of the three cases considered. When the smoothing function is steep, i.e., $n = 60$, it is clearly seen that the critical values converge better in the unit weight case. In addition to the Gibbs phenomenon mentioned above, this can be explained by the conservative properties of the Galerkin method with the unit weight function [2], which are altered when the Chebyshev or other non-unit weight is used. The absence of any numerical viscosity, even for the steep velocity gradients, can be a reason for the better convergence of unit weight discretization.

Several results obtained by other authors using other numerical methods (Table 2) also show a considerable disagreement. In our opinion the reason for the disagreement is the same, i.e., the discontinuity of the boundary conditions. This makes all the results dependent on the discretization of the flow region, as well as on the numerical scheme. Corresponding examples can be found in [21,23]. Note that for natural convection benchmarks reported below the agreement between different numerical methods, as well as between results computed with the different weight functions, is much better.

3.2. Convection of air in a square differentially heated cavity

This is one of the earliest CFD benchmark problems [25]. The first formulation considered steady convection of air ($Pr = 0.71$) in a square cavity whose horizontal walls are thermally insulated and vertical walls are maintained at different temperatures. The early benchmark exercise considered steady flow states for Rayleigh number $Ra = GrPr$ values ranging from 10^3 to 10^6. Later the range of the Rayleigh number was increased up to 10^8 [26–28] and to the calculation of the critical Rayleigh number corresponding to the onset of the oscillatory instability [10,29,30]. Here, we report results mainly for $Ra = 10^8$ and critical parameters corresponding to the onset of oscillatory instability. Results obtained by the described method for lower values of the Rayleigh number can be found in [1,4].

The streamlines and the isotherms of steady flow calculated at $Ra = 10^8$ are the same as in [26] and are not reported here. The pressure calculated using Eq. (5) is shown in Fig. 3 for the Rayleigh number varying from 10^3 to 10^8. The isobars are qualitatively similar to those reported in [26,28], however quantitative comparison is not possible, since no numerical values were reported in these papers. The isobars are equally spaced. The minimal and maximal values of the pressure are shown on the corresponding graphs. Other characteristic values chosen for the comparison in [25] are shown in Table 3, where the present results are compared with other data. The reader is referred to [25] for the description of all the parameters compared. A comparison with the very precise results of [26] shows that there is no advantage in the accuracy of solution if the divergent (18) or stream-function formulation (21) with the Chebyshev weight applied. Comparison of the results obtained with the unit, mixed and Chebyshev weight functions does not show a significant difference in the properties calculated in the central part of the cavity. However, the Chebyshev weight function yields the values of $V_{\max}$ and Nu which are in better agreement with the results of [26], than the values calculated with the unit weight. This is the effect of the Chebyshev weight function, which grows rapidly near the boundaries, and therefore yields better approximation of thin boundary layers located near the vertical boundaries.

The effect of the Chebyshev weight near the boundary is illustrated in Fig. 4 showing the convergence of the Nusselt number with increasing number of the basis functions for $Ra = 10^6$, 10^7 and 10^8. It is seen that at these rather large values of the Rayleigh number the approximation yielded by a smaller number of the

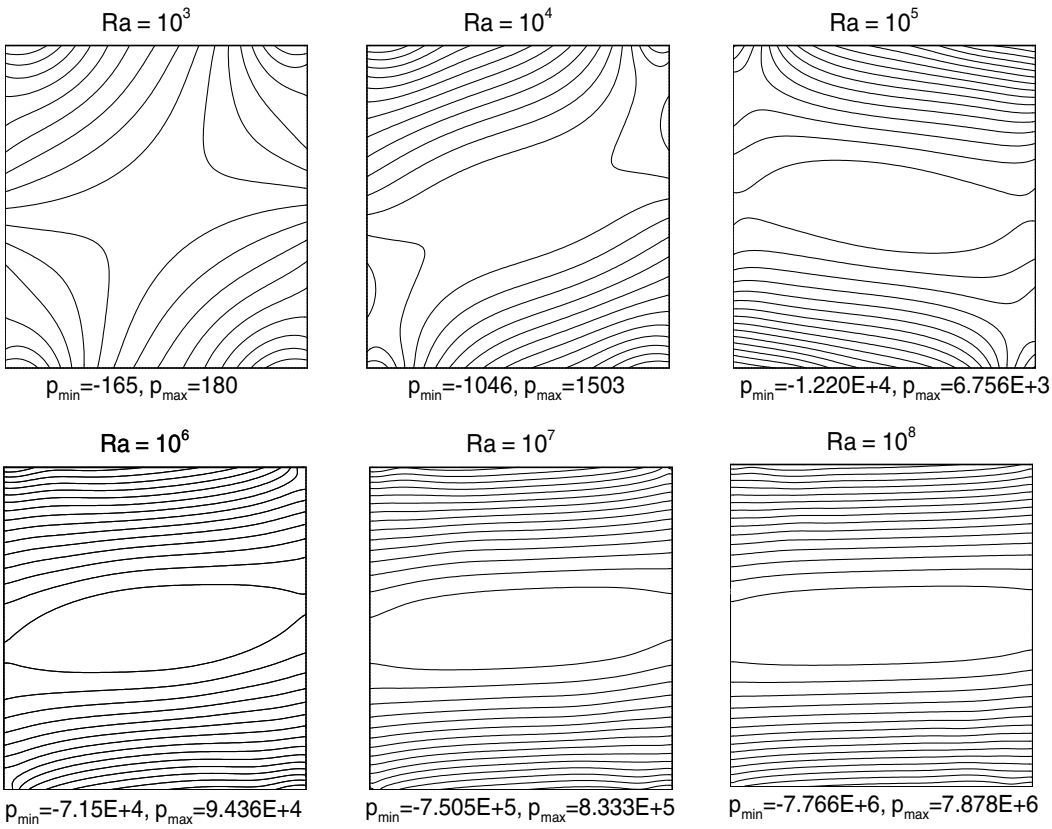

Fig. 3. Isobars of air convection in a differentially heated square cavity at different Rayleigh numbers. $Pr = 0.71$.

basis functions is better when the Chebyshev weight is applied. The use of Chebyshev weight leads to a slightly faster convergence. Obviously, the converged results obtained with a large number of the basis functions do not differ. No visible difference in the results obtained with the unit or mixed weight is observed (Fig. 4).

The better convergence of the Nusselt number with the use of the Chebyshev weight should be attributed to the projections of the energy rather than the momentum equation. This was checked by making the projections of the momentum equation with the unit weight and projections of the energy equations with the Chebyshev weight. The calculated Nusselt numbers coincided to within the fifth decimal digits with those calculated with the use of the Chebyshev weight in all the equations. However, the effect of the Chebyshev weight on the momentum equation is clearly seen when other properties of the flow are studied. An example of that is given in Fig. 5 showing the convergence of the maximal value of the stream function at $Ra = 10^8$. Note, that the maximum of the stream function is located close to the sidewall boundary layer, but not inside it (Table 3). For this property the convergence yielded by the mixed weight is the most monotonic. Thus, for this particular case, the use of the Chebyshev weight for the momentum equation and the unit weight in the pressure and energy equations yields a better approximation of the flow field.

The critical Rayleigh number and the critical oscillation frequency calculated with 64×64 basis functions are compared with the results of [10,30] in Table 4. Following the definitions used in [29,30] the frequency is made dimensionless by $H^2/\alpha\sqrt{Ra}$, where α is the thermal diffusivity. Similar to the characteristic values of the steady flows, the use of the Chebyshev weight yields results, that are closer to those calculated

Table 3
Results for convection of air in a square cavity with adiabatic horizontal walls. $Ra = GrPr = 10^8$, $Pr = 0.71$

	Present results, 60×60 basis functions					Independent results		
	($\mathbf{v}$,p)-Formulation, unit weight	($\mathbf{v}$,p)-Formulation, mixed weight	($\mathbf{v}$,p), Chebyshev weight, $\mathbf{v}\cdot\nabla\mathbf{v}$	($\mathbf{v}$,p)-Formulation Chebyshev weight, $\mathbf{v}\times[\nabla\times\mathbf{v}]$	ψ-Formulation, Chebyshev weight	[27], 70×70 non-uniform bilinear finite element grid	[26], 72×72 Chebyshev pseudospectral modes	[28], h-adaptive finite element grid
$\psi\left(\frac{1}{2},\frac{1}{2}\right)$	52.3223	52.3181	52.3221	52.3221	52.3245		52.3223	
$\psi_{\max}$	53.8482	53.8440	53.8480	53.8479	53.8504		53.8475	
$X_{\max}$ ($\psi_{\max}$)	0.048266	0.048269	0.048265	0.048265	0.048266		0.048	
$Y_{\max}$ ($\psi_{\max}$)	0.552531	0.552594	0.552587	0.552587	0.552504		0.553	
$U_{\max}$	321.8615	321.8710	321.5864	321.514	321.8210	315.2603	321.875	283.0689
$Y_{\max}$ ($U_{\max}$)	0.927834	0.9278503	0.9277077	0.9277000	0.9277994	0.9389	0.928	0.9455
$V_{\max}$	2222.2892	2222.0324	2222.3879	2222.3855	2222.5000	2241.1841	2222.39	2223.4424
$X_{\max}$ ($V_{\max}$)	0.012000	0.012000	0.012000	0.012000	0.012000	0.0136	0.012	0.0130
Nu ($x = 0$)	30.22748	30.22503	30.22561	30.22561	30.22585	30.1901	30.225	29.6256

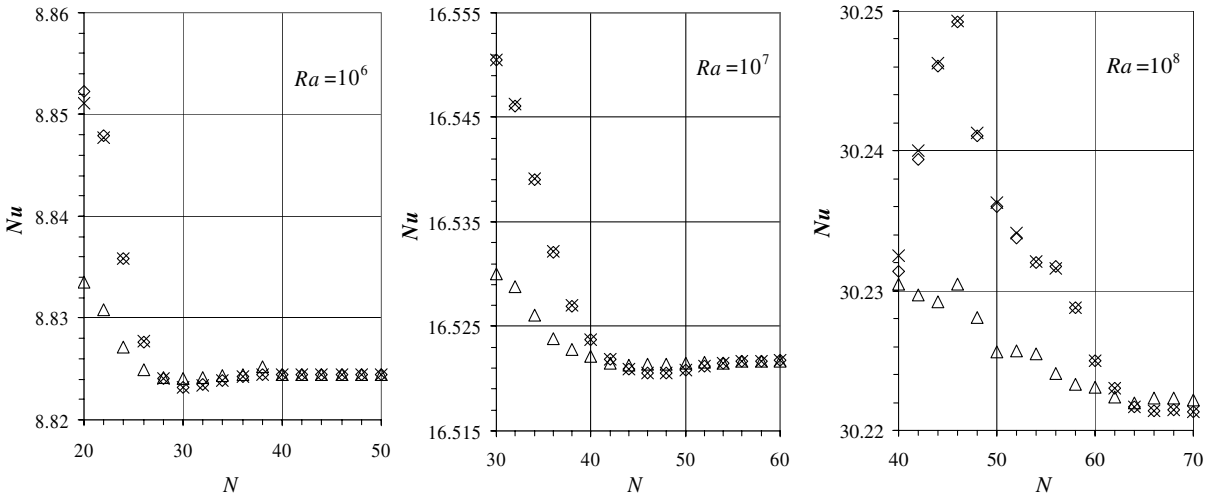

Fig. 4. Convection of air in differentially heated square cavity with adiabatic horizontal walls. Convergence of the Nusselt number. $Pr = 0.71$, $N = N_x = N_y$. ×, unit weight; ◇, mixed weight; △, Chebyshev weight.

in other studies. The convergence of critical parameters for the four variations of the weight functions is shown in Fig. 6. It should be noted that the correct perturbation pattern can be obtained only for $N \geqslant 40$. The converged second decimal digit of the critical parameters can be obtained only for $N \geqslant 50$, and the third for $N \geqslant 58$. The values of Ra_{cr} shown for $N < 40$ correspond to the perturbations with incorrect spatial pattern. The values of the corresponding critical frequencies for $N < 40$ are beyond the value of 0.05 and are not shown.

It can be concluded that the effect of the Chebyshev weight will be most noticeable in flows containing thin boundary layers. This is illustrated by the two following examples. In the first example we consider again the

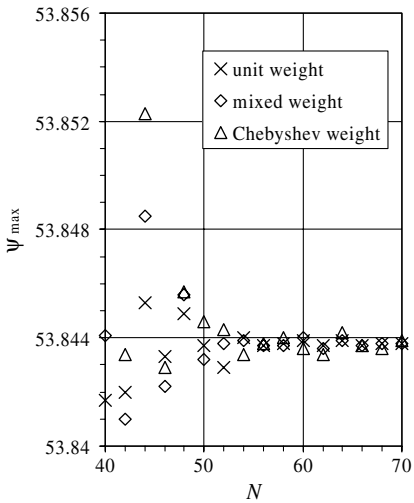

Fig. 5. Convection of air in differentially heated square cavity with adiabatic horizontal walls. Convergence of the maximal value of stream function and the Nusselt number. $Ra = 10^8$, $Pr = 0.71$, $N = N_x = N_y$.

Table 4
Critical Rayleigh number and critical oscillation frequency for convection of air in a square cavity with adiabatic horizontal walls

Reference	Discretization	$Ra_{cr} \times 10^{-8}$	f_{cr}
[10]	54×56 Galerkin basis functions	1.83	0.04645
[30]	72×72 pseudospectral modes	1.84	0.045
Present			
Unit weight	64×64 basis functions	1.824	0.04655
Chebyshev weight	64×64 basis functions	1.828	0.04650
Mixed weight	64×64 basis functions	1.824	0.04655
Chebyshev weight in the energy equation only	64×64 basis functions	1.827	0.04650

convection of air in a laterally heated square cavity, but we replace the perfectly insulating boundaries by perfectly conducting ones. This leads to elimination of the boundary layers [1,29], and as a result, to much faster convergence of the Galerkin method. The calculations with the unit weight converge slightly faster, but beyond $N = 24$ the results obtained with different weight functions coincide to within the fourth decimal digit, and beyond $N = 46$ seven decimal digits remain unchanged with the further increase of the number of the basis functions. The converged result for this case is $Ra_{cr} = 2.108077 \times 10^6$ and $f_{cr} = 0.2136605$.

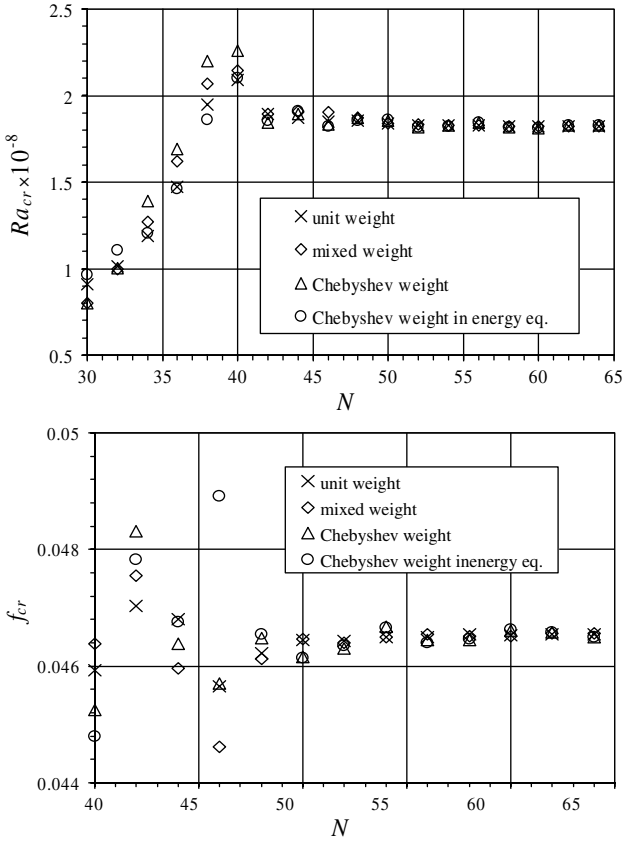

Fig. 6. Convection of air in laterally heated square cavity with adiabatic horizontal walls. Convergence of the critical Reynolds number and the critical frequency. $Pr = 0.071$, $A = 1$. $N = N_x = N_y$.

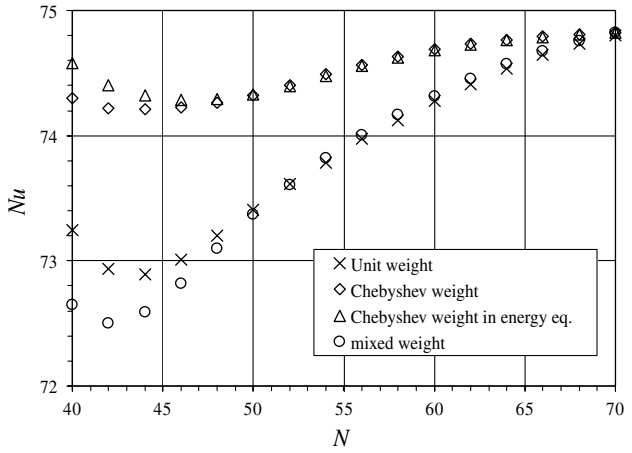

Fig. 7. Convection of water in differentially heated square cavity with adiabatic horizontal walls. Convergence of the Nusselt number. $Pr = 7$, $Gr = 4 \times 10^8$, $Ra = GrPr = 2.8 \times 10^9$, $N = N_x = N_y$.

An opposite example is shown in Fig. 7. Here, we consider the convection in a laterally heated square cavity with the perfectly insulated horizontal walls and increase the Prandtl number by a factor of 10 to $Pr = 7$, which corresponds to water. The increase of the Prandtl number leads to a thinning of the boundary layers adjacent to the vertical walls. As a result the Galerkin method converges extremely slowly. Fig. 7 shows that in this case the Chebyshev weight yields a significantly faster convergence. The implementation of the Chebyshev weight is more crucial for the energy equation since thermal boundary layers are thinner than the hydrodynamic ones. This is clearly seen from the comparison of the results obtained with the use of the Chebyshev weight for the whole problem and for the energy equation only with two other cases where the unit weight was used for the projections of the energy equation. For this case we were unable to calculate the converged value of the critical Rayleigh number.

3.3. Other natural convection benchmarks

Other benchmark problems dealing with the natural convection flows were formulated in [31,32]. Both benchmarks considered the onset of the oscillatory instability of convective flows in laterally heated rectangular cavities. Here we briefly report results of the calculations for these benchmarks using the unit and Chebyshev weight functions.

The benchmark problem of [31] was formulated for convection of a low-Prandtl-number fluid in a long horizontal cavity with length over height aspect ratio $A_h = L/H = 4$. Details on the results for this benchmark can be found in [1,4,31] and references therein. The present calculations were done for $N = N_x = 2N_y$ basis functions, where N was varied from 32 to 60. The flow under study has no boundary layers, thus the use of the Chebyshev weight does not improve the convergence. We observe that beyond $N = 50$ the results obtained with the Chebyshev and unit weight coincide. At smaller truncation numbers the results obtained with the unit weight are slightly better.

The benchmark problem formulated in [32] considers convection of air in a tall vertical cavity with the height over length ratio $A = H/L = 8$. The details of this benchmark can be found in [32,33], and the results obtained by the Galerkin method used here are reported in [5]. Only unit weight was used in [5]. The calculations were performed with a fixed number of the basis functions in the vertical direction $N_y = 100$, and varying the number of basis functions in the horizontal direction N_x. In this case all combinations of the unit and Chebyshev weight functions yield results that converge to the same value for $N_x > 20$. It can be

shown that like in the case of the square cavity the Chebyshev weight yields slightly better approximation of the Nusselt number calculated at the hot wall, where thermal boundary layer develops. At the same time the unit weight yields slightly better approximation of the velocity field.

4. Concluding remarks

A numerical treatment of the incompressible Navier–Stokes equation based on the global Galerkin method with the divergence free basis functions proposed in [1,2] for the unit weight function is extended to an arbitrary weight in the definition of the inner products. It is shown that the pressure can be eliminated by a straightforward procedure, so that resulting dynamical ODEs system contains no algebraic constraints. It is shown also how the pressure field can be calculated using the previously calculated velocity field. The approach can be extended to a more general method of weighted residuals.

Using the proposed approach several benchmark problems were solved with the use of the unit and Chebyshev weight functions, as well as their combinations. The results illustrate the applicability and robustness of the proposed pressure elimination. It was shown that discontinuities of boundary conditions make it disadvantageous to use the Chebyshev weight. At the same time the Chebyshev weight function yields better approximations of the boundary layers, as was shown for the convection of air and water in square cavity.

The present study can be continued in two directions. First, a successful use of the Chebyshev weight function may allow one to formulate an efficient pseudospectral technique for the integration of the resulting ODEs systems in time. Taking into account that no implicit pressure-calculation step is involved, this can yield an effective numerical method for the modeling of three-dimensional flows in simple domains such as rectangular boxes and cylinders. Another direction is a search for an algorithm for the adaptation of the weight function to a certain problem. An example of such an adaptation is given in Appendix A. This can lead to a significant improvement of the convergence and, consequently, to fewer degrees of freedom in the numerical method. This is extremely important both for stability studies and for the calculation of time-dependent 3D flows at large Reynolds numbers.

Acknowledgements

This study was supported by the German-Israeli Foundation, Grant No. 1-794-145.10/2004. The author would like to acknowledge the use of computer resources of the High Performance Computing Unit, a division of the Israel Inter University Computing Center.

Appendix A

Here, we illustrate how the weight function can be adopted to a certain problem. To do this we consider the time-dependent problem for the Burgers equation [34]:

$$\frac{\partial u}{\partial t} + u\frac{\partial u}{\partial x} = v\frac{\partial^2 u}{\partial x^2} \tag{A1}$$

with the boundary conditions $u(0,t) = u(1,t) = 0$, and the initial condition $u(x,0) = \sin(2\pi x) + \sin(\pi x)/2$ as defined in [35]. Eq. (A1) is discretized by the Galerkin method using the decomposition

$$u(x,t) = \sum_{i=0}^{N-1} c_i(t)[T_i(x) - T_{i+2}(x)] \tag{A2}$$

and the inner product defined as

$$\langle f, g\rangle = \int_0^1 (x - x^2)^{-\alpha} f(x) g(x)\,\mathrm{d}x \approx \frac{1}{M}\sum_{i=1}^{M} (x_i - x_i^2)^{-\alpha+1/2} f(x_i) g(x_i). \tag{A3}$$

The last approximate equality is the Gauss quadrature formula, which is applied over $M = 300$ points $x_i = [1 + \cos(\pi(2i - 1)/2M)]/2$. Note, that the integral in Eq. (A3) converges for finite $f(x)$ and $g(x)$ if $\alpha < 1$. However, α can be larger if these functions vanish at $x = 0$ and 1, as in the present example. The time integration is carried out using the ODEPACK routines [36]. Apparently, $\alpha = 0$ corresponds to the unit, and $\alpha = 0.5$ to the Chebyshev weight.

For the following analysis, we solve this problem for $\nu = 0.01$ and integrate in time until $t = 0.2$. To obtain a reference solution $u_{\mathrm{ref}}(x)$ we use $N = 300$. For this truncation number two solutions obtained using the unit and Chebyshev weight functions are practically indistinguishable. Then we reduce the truncation number to $N = 100$ and monitor the relative residual

$$r = \max_x \left| \frac{u_N(x) - u_{\mathrm{ref}}(x)}{u_{\mathrm{ref}}(x)} \right|, \tag{A4}$$

Table 5
The relative deviation from the reference solution r versus the power α of the weight function $\rho(x) = (x - x^2)^{-\alpha}$ for a solution of the Burgers equation with 100 basis functions

α	0	0.5	1	1.1	1.2	1.3	1.4	1.5	2
$r \times 10^3$	5.54	0.979	0.265	0.16	0.0793	0.0193	0.0241	0.0548	0.108

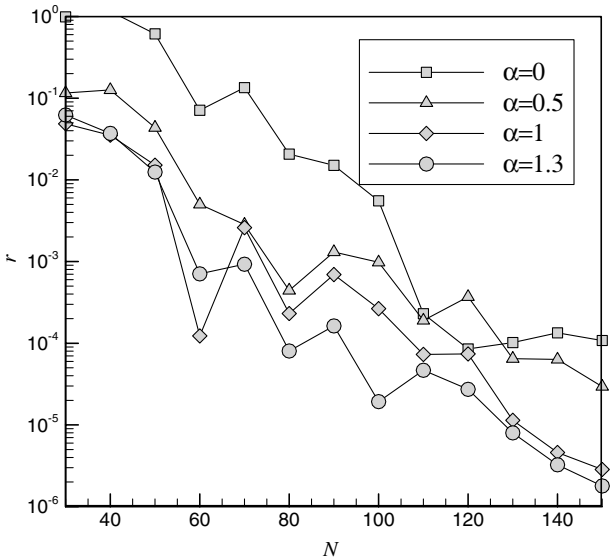

Fig. 8. Relative residual r of the numerical solution of the Burgers equation (A1) versus the truncation number N for different weight function parameter α.

where $u_N(x)$ is the numerical solution corresponding to the truncation number N. The result for different α is shown in Table 5. It is seen that the residual reaches its minimum at $\alpha = 1.3$, for which it is almost two orders of magnitude less than for the Chebyshev weight at $\alpha = 0.5$. Fig. 8 shows how the relative residual r vanishes with variation of the truncation number of series (A2) for different values of α. It is seen that beyond $N = 80$ the residual corresponding to the adapted value $\alpha = 1.3$ remains significantly smaller than that of the unit ($\alpha = 0$) or Chebyshev ($\alpha = 0.5$) weight functions, as well as smaller than the residual corresponding to $\alpha = 1$. It is emphasized that the optimal value of α obtained for $N = 100$ remains optimal for larger truncation numbers, at least up to $N = 150$.

References

[1] A.Yu. Gelfgat, I. Tanasawa, Numerical analysis of oscillatory instability of buoyancy convection with the Galerkin spectral method, Numer. Heat Transfer Pt. A. 25 (1994) 627.
[2] A.Yu. Gelfgat, Two- and three-dimensional instabilities of confined flows: numerical study by a global Galerkin method, Comput. Fluid Dynam. J. 9 (2001) 437.
[3] A.Yu. Gelfgat, Different modes of Rayleigh–Bénard Instability in two- and three-dimensional rectangular enclosures, J. Comput. Phys. 156 (1999) 300.
[4] A.Yu. Gelfgat, P.Z. Bar-Yoseph, A.L. Yarin, Stability of multiple steady states of convection in laterally heated cavities, J. Fluid Mech. 388 (1999) 315.
[5] A.Yu. Gelfgat, Stability and slightly supercritical oscillatory regimes of natural convection in a 8:1 cavity: solution of benchmark problem by a global Galerkin method, Int. J. Numer. Meth. Fluids 44 (2004) 135.
[6] A. Gelfgat, P.Z. Bar-Yoseph, A. Solan, Stability of confined swirling flow with and without vortex breakdown, J. Fluid Mech. 311 (1996) 1.
[7] A.Yu. Gelfgat, P.Z. Bar-Yoseph, A. Solan, Three-dimensional instability of axisymmetric flow in a rotating lid – cylinder enclosure, J. Fluid Mech. 438 (2001) 363.
[8] L.S. Tuckerman, Divergence-free velocity fields in nonperiodic geometries, J. Comput. Phys. 80 (1989) 404.
[9] J.M. Lopez, J. Shen, An efficient spectral-projection method for the Navier–Stokes equations in cylindrical geometries. I. Axisymmetric cases, J. Comput. Phys. 139 (1998) 308.
[10] H. Yahata, Stability analysis of natural convection in vertical cavities with lateral heating, J. Phys. Soc. Jpn. 68 (1999) 446.
[11] A. Meseguer, F. Marques, On the competition between centrifugal and shear instability in spiral Couette flow, J. Fluid Mech. 402 (2000) 33.
[12] S.A. Suslov, S. Paolucci, A Petrov–Galerkin method for the direct simulation of fully enclosed flows, Proc. ASME Heat Transfer Division HTD 335 (1996) 39.
[13] S.A. Suslov, S. Paolucci, A Petrov–Galerkin method for flows in cavities: enclosure of aspect ratio 8, Int. J. Numer. Meth. Fluids 40 (2002) 999.
[14] P.M. Gresho, R.L. Sani, On pressure boundary conditions for the incompressible Navier–Stokes equations, Int. J. Numer. Meth. Fluids 7 (1987) 1111.
[15] D. Rempfer, Low-dimensional modeling and numerical simulation of transition in simple shear flows, Annu. Rev. Fluid Mech. 35 (2003) 229.
[16] O. Botella, R. Peyret, Benchmark spectral results on the lid-driven cavity flow, Comput. Fluids 27 (1998) 421.
[17] N. Ramanan, G.M. Homsy, Linear stability of lid-driven cavity flow, Phys. Fluids 6 (1994) 2690.
[18] S. Albensoeder, H.C. Kuhlmann, H.J. Rath, Three-dimensional centrifugal-flow instabilities in the lid-driven cavity problem, Phys. Fluids 13 (2001) 121.
[19] M. Poliashenko, C.K. Aidun, A direct method for computation of simple bifurcations, J. Comput. Phys. 121 (1995) 246.
[20] J.J. Gervais, D. Lemelin, R. Pierre, Some experiments with stability analysis of discrete incompressible flows in the lid-driven cavity, Int. J. Numer. Meth. Fluids 24 (1997) 477.
[21] A. Fortin, M. Jardak, J.J. Gervais, R. Pierre, Localization of Hopf bifurcations in fluid flow problems, Int. J. Numer. Meth. Fluids 24 (1997) 1185.
[22] F. Auteri, N. Parolini, L. Quartapelle, Numerical investigations on the stability of singular driven cavity flow, J. Comput. Phys. 183 (2002) 1.
[23] Y.-F. Peng, Y.-H. Shiau, R.R. Hwang, Transition in a 2-D lid-driven cavity flow, Comput. Fluids 32 (2003) 337.
[24] M. Sahin, R.G. Owens, A novel fully-implicit finite volume method applied to the lid-driven cavity problem. Part. II. Linear stability analysis, Int. J. Numer. Meth. Fluids 42 (2003) 79.

[25] G. de Vahl Davis, I.P. Jones, Natural convection in a square cavity: a comparison exercise, Int J. Numer. Meth. Fluids 3 (1983) 227.
[26] P. Le Quéré, Accurate solutions to the square thermally driven cavity at high Rayleigh number, Comput. Fluids 20 (1991) 29.
[27] N. Kondo, Numerical simulation of unsteady natural convection in a square cavity by the third-order upwind finite element method, CFD J. 3 (1994) 281.
[28] D.A. Mayne, A. Usmani, M. Crapper, h-adaptive finite element solution of high Rayleigh number thermally driven cavity problem, Int. J. Numer. Meth. Heat Fluid Flow 10 (2000) 598.
[29] R.A.W.M. Henkes, P. Le Quéré, Three-dimensional transition of natural convection flows, J. Fluid Mech. 319 (1996) 281.
[30] P. Le Quéré, M. Behnia, From onset of unsteadiness to chaos in a differentially heated square cavity, J. Fluid Mech. 359 (1998) 81.
[31] B. Roux (Ed.), Numerical Simulation of Oscillatory Convection in Low-Pr Fluids: A GAMM workshop, Notes on Numerical Fluid Mechanics, vol. 27, Vieweg, Braunschweig, 1990.
[32] M.A. Christon, P.M. Gresho, S.B. Sutton, Computational predictability of time-dependent natural convection flows in enclosures including benchmark solution, Int. J. Numer. Meth. Fluids 40 (2002) 953.
[33] S. Xin, P. Le Quéré, An extended Chebyshev pseudo-spectral benchmark for the 8:1 differentially heated cavity, Int. J. Numer. Meth. Fluids 40 (2002) 981.
[34] C. Basdevant, M.O. Deville, P. Haldenwang, J.M. Lacroix, J. Ouazzani, R. Peyret, P. Orlandi, A.T. Patera, Spectral and finite difference solutions of the Burgers equation, Comput. Fluids 14 (1986) 23.
[35] W. Huang, Y. Ren, R.D. Russel, Moving mesh methods based on moving mesh partial differential equations, J. Comput. Phys. 113 (1994) 279.
[36] C. Hindmarsh, ODEPACK A Systematized Collection of ODE Solvers, in: R.S. Stepleman et al. (Eds.), Scientific Computing, vol. 1, North-Holland, Amsterdam, 1983, pp. 55–64.